Volume 13 | Number 44 | 28 November 2015 | Pages 10765–10958

Organic & Biomolecular Chemistry

www.rsc.org/obc

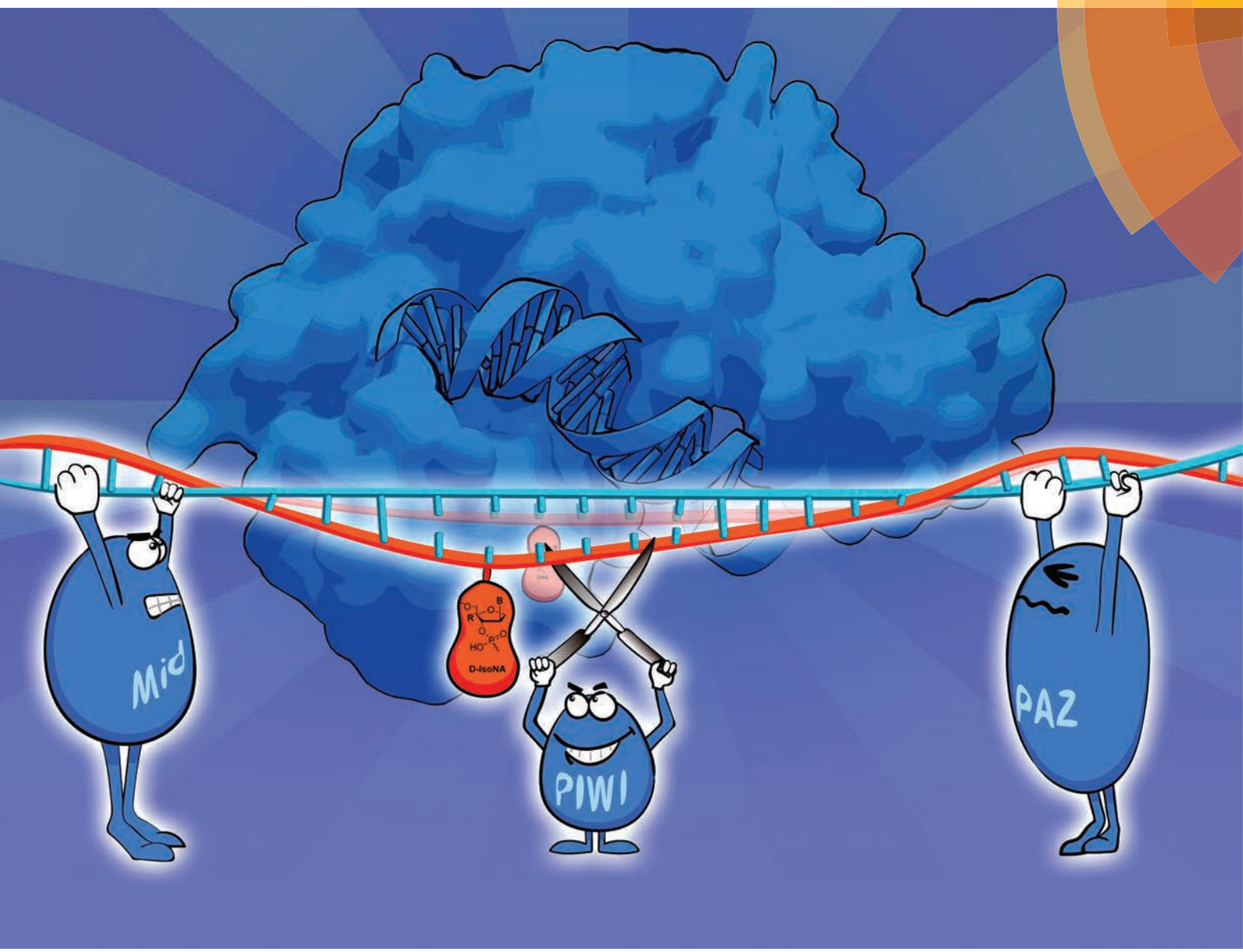

ISSN 1477-0520

ROYAL SOCIETY OF CHEMISTRY

PAPER

Yi-Lei Zhao, Zhenjun Yang *et al.*

D-Isonucleotide (isoNA) incorporation around cleavage site of passenger strand promotes the vibration of Ago2-PAZ domain and enhances *in vitro* potency of siRNA

Organic & Biomolecular Chemistry

PAPER

View Article Online
View Journal | View Issue

Cite this: *Org. Biomol. Chem.*, 2015, **13**, 10825

D-Isonucleotide (isoNA) incorporation around cleavage site of passenger strand promotes the vibration of Ago2-PAZ domain and enhances *in vitro* potency of siRNA

Ye Huang,†[a,e] Miao Tian,†[a] Yichao Zhang,[b] Gang Sheng,[c] Zhuo Chen,[a] Yuan Ma,[a] Yue Chen,[a] Yihong Peng,[d] Yi-Lei Zhao,*[b] Yanli Wang,[c] Lihe Zhang[a] and Zhenjun Yang*[a]

Received 4th June 2015,
Accepted 11th August 2015

DOI: 10.1039/c5ob01119a

www.rsc.org/obc

It has been demonstrated that passenger strand cleavage is important for the activation of RNA-induced silencing complex (RISC), which is a crucial step for siRNA-mediated gene silencing. Herein, we report that isonucleotide (isoNA) modification around the cleavage site of the passenger strand would affect the *in vitro* potency of modified siRNAs by altering the motion pattern of the Ago2-PAZ domain. According to western blotting, q-PCR and antiviral test results, we proved that D-isonucleotide (isoNA) modification at the position 8 of the passenger strand (siMek1-S08D), which is adjacent to the cleavage site, markedly improved the *in vitro* potency of the modified siRNA, whereas siRNAs with D-isoNA incorporation at position 9 (siMek1-S09D) or L-isoNA incorporation at positions 8 and 9 (siMek1-S08L, siMek1-S09L) displayed lower activity compared to native siRNA. Kinetics evaluation of passenger strand cleavage induced by *T. thermophilus* Ago (Tt-Ago) showed that D-isoNA modification at position 8 of the passenger strand had no significant influence on the cleavage rate, but L-isoNA modification at position 8 slowed the cleavage rate markedly. Moreover, the results of molecular dynamics simulations showed that D-isoNA modification at position 8 affected the open-close motion of the PAZ domain in the Ago/siRNA complex, which may promote the loading of RISC and release of a passenger strand cleavage product, and consequently accelerate the activation of RISC and enhance silencing activity. However, D-isoNA modification at position 9 or L-isoNA modification at position 8 or 9 exerted opposite influences on the motion of the Ago-PAZ domain.

Introduction

Since the discovery of the RNA interference (RNAi) effect in *Caenorhabditis elegans*,[1] double-stranded small interfering RNA (siRNA) molecules have been proved to be able to exert a potent gene knockdown effect in mammalian cells[2] and other eukaryotes[3–5] Assembly of the RNA-induced silencing complex (RISC) is the pivotal step in the RNAi pathway.[6] In humans, a siRNA duplex with both guide strand and passenger strand is first recognized by the RLC complex, which contains Dicer and the RNA-binding protein TRBP, to form an immature RISC complex.[7] Then, the passenger strand is nicked between positions 9 and 10, counted from the 5′-terminal, by the Argonaute 2 (Ago2) protein in the same way as target mRNA is cleaved,[8,9] followed by being degraded by C3PO to finally activate the RISC.[10] Active RISC recognizes and cleaves complementary target RNA to execute the silencing process.

A dramatic reduction in the cleavage efficiency of target RNA was found when chemical modification occurred around the nicked site of the passenger strand. These chemical modifications may limit the formation of RISC and then impair the silencing activity of siRNA by blocking the cleavage of the passenger strand.[8,11] For example, replacing the phosphodiester linkage between position 9 and position 10 with phosphorothioate, modifying position 9 with 2′-*O*-methylribose, and introducing 4-nt mismatches from position 9 to position 11, all caused a great reduction in the cleavage efficiency of

[a]*State Key Laboratory of Natural and Biomimetic Drugs, School of Pharmaceutical Sciences, Peking University, Beijing 100191, China. E-mail: yangzj@bjmu.edu.cn*
[b]*State Key Laboratory of Microbial Metabolism, School of Life Sciences and Biotechnology, Shanghai Jiao Tong University, Shanghai, China. E-mail: yileizhao@sjtu.edu.cn*
[c]*Laboratory of Non-Coding RNA, Institute of Biophysics, Chinese Academy of Sciences, Beijing, China*
[d]*Department of Microbiology, School of Basic Medical Sciences, Peking University, Beijing, China*
[e]*Department of New Drug Research and Development, Institute of Materia Medica, Peking Union Medical College & Chinese Academy of Medical Sciences, Beijing, China*
†These authors contributed equally to this paper.

complementary target RNA. However, the same modifications that were positioned 1- or 2-nt downstream of the cleavage site or away from the central position did not affect the cleavage of target RNA.[11] On the other hand, when thermally destabilizing modifications were placed around the cleavage site of the passenger strand, an obvious enhancement in silencing activity was found.[12] This unusual phenomenon may be due to the fact that thermally destabilizing modifications change the regional conformation around the active site and assist the cleavage-related residues of Ago2 protein to interact with the phosphodiester bond between position 9 and position 10 of the passenger strand. All these reports indicate that alteration of the conformation around the cleavage site of the passenger strand may affect the silencing activity.

Isonucleotide (isoNA) (Fig. 1A) is a novel type of nucleotide analogue in which the nucleobase is moved to another position of ribose other than C-1′.[13,14] In our previous study, we found that isonucleotide modification could alter the regional conformation around the incorporation site when modified DNA or RNA oligonucleotides were hybridized with a complementary DNA/RNA strand. For example, L-isoNA modification at the 3′-terminus of DNA oligonucleotides created a conformation that blocked exonuclease recognition and then increased their exonuclease-resistant ability, whereas L-isoNA modification in the middle of oligonucleotides altered the regional conformation into a form that is more suitable for RNase H recognition and then promoted the degradation of complementary RNA.[15–17] Then, we reported that D-isoNA and L-isoNA incorporation could introduce regional conformation alteration into a siRNA duplex and affect the physicochemical and biological properties at varying degrees.[18] Therefore, D-/L-isoNA could be applied as a pair of chemical tools to investigate the systematic relationship between conformational alteration around every single nucleotide of siRNA and their biological potency.

Through thermal denaturation and dynamic simulation studies, we have demonstrated that D-isoNA and L-isoNA modification at positions 8 and 9 of the passenger strand would affect the original compact duplex by introducing flexible conformations of different degrees.[18] Therefore, in this study, further silencing activity, antivirus activity and dynamic simulation studies were applied to thoroughly explore the influence

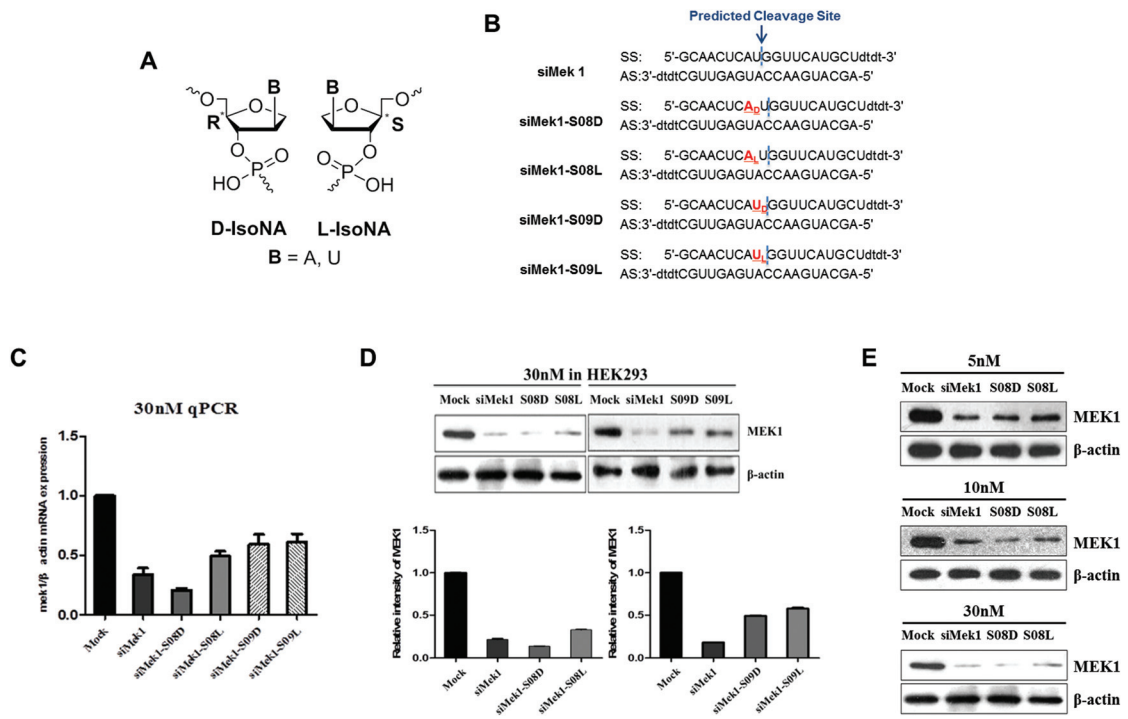

Fig. 1 Silencing activity affected by D-/L-isoNA modification at positions 8 and 9 of passenger strand. (A) Structures of D-isonucleotide (D-isoNA, left) and L-isonucleotide (L-isoNA, right). (B) Sequences of siMek1s modified with D-isoNA or L-isoNA in the passenger strand. The blue dotted lines represent the predicted cleavage sites. (C) Quantitative PCR results of mek1 mRNA. HEK293 cells were co-transfected with siMek1 and siMek1s modified with D-isoNA or L-isoNA in the passenger strand at 30 nM of each. Mek1 mRNA was measured 24 h later by quantitative PCR. Mek1 mRNA levels were normalized to β-actin mRNA, which was used as a loading control. The uninhibited normalized mek1 mRNA level was set to 100%. The data are the average of three independent experiments and error bars denote the standard deviations. (D) Western blotting analysis of MEK1 protein. HEK293 cells were co-transfected with siMek1 and siMek1s modified with D-isoNA or L-isoNA in the passenger strand at 30 nM of each. Protein lysates were prepared for 36 h and blotted with MEK1 antibodies. Quantification of mek1 bands was normalized by densitometric scanning of actin using the Band Leader software (version 3.0). The relative intensity of MEK1 on the *y*-axis is represented by the percentage of the intensity of mock transfection (100%). The data are the average of three independent experiments and error bars denote the standard deviations. (E) Western blotting analysis of MEK1 protein when HEK293 cells were co-transfected with siRNAs at 5 nM, 10 nM, and 30 nM.

of regional conformation alteration caused by D-/L-isoNA modification on the process of passenger strand cleavage and the silencing potency of modified siRNAs. The siRNA sequence that targets the MEK1 kinase mRNA, which is crucial for the replication process of various common viruses, was chosen for the further evaluation of silencing activity and antivirus activity *in vitro* (Fig. 1B).[19,20]

Results

Silencing activity affected by D-/L-isoNA incorporation at positions 8 and 9 of passenger strand

Quantitative PCR and western blotting were utilized to investigate the silencing activity of the synthesized siRNAs with D-/L-isoNA modification at passenger strand at RNA level and protein level, respectively, in a HEK293 cell line. According to the results of qPCR evaluation, when position 8 on the passenger strand was replaced with D-isoNA (siMek1-S08D), greater silencing potency than the native sequence was found; on the contrary, L-isoNA at the same position 8 (siMek1-S08L) impaired the silencing potency. However, at the position 9, both D-isoNA and L-isoNA exhibited decreased silencing activity, although the degree of decreasement was not as obvious as siMek1-S08L (Fig. 1C). This same phenomenon was also found at protein level, namely, S08D exhibited the strongest knockdown effect, whereas S08L exhibited worse effect than the native sequence. D-/L-isoU modification at the position 9 showed decreased silencing activity compared to the native sequences and the difference was more obvious at protein level (Fig. 1D). The difference between the silencing activities of siMek1-S08D, siMek1-S08L and native siMek1 were nearly the same at three different concentrations of siRNA, namely, 5 nM, 10 nM, and 30 nM. This indicated that siMek1-S08D provided the best silencing activity regardless of the concentration, although the degree of enhancement was not obvious when the concentration of siRNA was too low, such as 5 nM (Fig. 1E). In a word, D-isoNA modification at the position 8 of the passenger strand was able to enhance the *in vitro* potency of siRNA.

Influence of modification with isoNA on the kinetics of passenger strand cleavage induced by *T. thermophilus* Ago (Tt-Ago)

According to the results of the evaluation of silencing activity, modification with D-isoNA at the position 8 of the passenger strand may improve the silencing effect of siRNA. Conversely, other modification strategies around this area, such as the incorporation of L-isoNA at the same position or D-/L-isoNA at the adjacent position 9, would impair the activity. In previous reports, the chemical modifications that disturb cleavage of the passenger strand were found to be able to impair the silencing activity of siRNA by limiting the formation of RISC.[11] This reminds us that modification with isoNA around the cleavage site of the passenger strand may also modulate silencing activity by directly affecting the efficiency of the cleavage process or other steps. Therefore, the influence of modification with isoNA on the kinetics of passenger strand cleavage induced by *T. thermophilus* Ago (Tt-Ago) was evaluated. Previous reports studied the cleavage kinetics of the passenger strand with a 5′-^{32}P-radiolabeled RNA oligonucleotide.[11] They detected the cleavage fragment of the passenger strand *via* autoradiography imaging of ^{32}P. However, the labelling process using ^{32}P is complicated, time-consuming and dangerous. Herein, we detected the cleavage fragment with 3′-terminal-Cy3-labelled passenger RNA instead of a 5′-^{32}P-radiolabeled RNA oligonucleotide. To avoid the influence caused by the steric hindrance of the Cy3 group on RISC activation, four extra uridine nucleotides were added at the 3′-terminus (Fig. 2A).

According to the results of cleavage kinetics (Fig. 2B), when D-isoNA and L-isoNA were incorporated at positions 8 and 9 of the passenger strand, neither of them disturbed the cleavage process dramatically. The cleavage of all five 3′-Cy3-labelled RNA strands, Cy3-MKS-23, Cy3-MKS-2308D, Cy3-MKS-2308L, Cy3-MKS-2309D, and Cy3-MKS-2309L, started after 30 min and finished after 120 min. However, according to the fluorescence intensity at 60 min, we found that modification with D-isoNA affected the cleavage process lesser than modification with L-isoNA. Cy3-MKS-2308D and Cy3-MKS-2309D had nearly the same cleavage rate as Cy3-MKS-23, but the cleavage of Cy3-MKS-2308L and Cy3-MKS-2309L was slower. This indicated that the low silencing activity of S08L and S09L may be due to the disturbance caused by L-isoNA incorporation to the interaction between the PIWI domain of Ago and the cleavage site of passenger RNA. In addition, the stronger silencing activity of S08D could not be simply explained through the cleavage kinetics experiment.

Stability of the Ago/siRNA complexes and change in motion of Ago functional domains

Then, the mechanism of this difference was investigated by molecular dynamics simulations. RMSF of five simulated models of a complex of Ago2 and siRNAs are shown in Fig. 3A. In the Ago_Native model with no modifications, there are two loops that are obviously flexible. As shown in Fig. 3B, the two loops belong to two different functional domains, PAZ and PIWI, and the PAZ loop is more flexible than the PIWI loop. After isoNA modifications, the flexibility of the two loops decreased, especially for the PAZ loop. Ago_S08D model exhibited the smallest decrease, whereas Ago_S08L displayed the largest decrease. For the siRNA part, there was no detectable change in flexibility.

The four different domains of the Ago protein have crucial functions in the cleavage process. We found that the flexibility of the PAZ and PIWI domains changed after isoNA modification, but there is no information regarding how the motions of the domains vary. Principle component analysis (PCA) was performed on the Ago/siRNA models to reveal the significant transformations of the functional domains. From the PC1 in Ago_Native model (Fig. 3D), we found an obvious open-close motion for the PAZ loop, which is in accordance with the RMSF result and is also found in other molecular dynamics

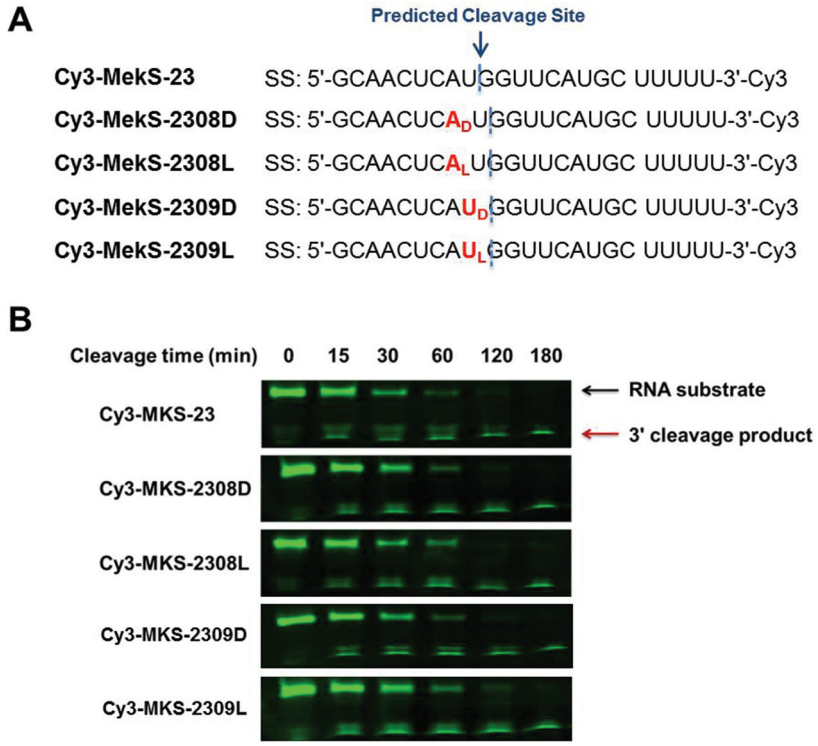

Fig. 2 Influence of isoNA modification on the kinetics of passenger strand cleavage induced by *T. thermophilus* Ago (Tt-Ago). (A) Sequences of 3′-Cy3-labeled D-/L-isoNA-modified siRNA. (B) Kinetics of passenger strand cleavage induced by *T. thermophilus* Ago (Tt-Ago). Reaction buffer: 10 mM Hepes (pH = 7.5), 100 mM NaCl, 5 mM $MnCl_2$; 5 μM Tt-Ago and 5 μM guide DNA strand, incubation at 42 °C for 30 min; then, 3 μM passenger RNA strand was added and the incubation temperature was increased to 70 °C for cleavage reaction; the cleavage mixtures were sampled at 0 min, 15 min, 30 min, 60 min, 120 min, and 180 min, and separated on a 20% PAGE gel with cleavage fragments and visualized under fluorescent light. The black arrow points at the intact passenger RNA substrate and the red arrow points at the 3′-cleavage passenger RNA fragment.

simulations. The open-close motion of the PAZ loop is thought to be important for the propagation of the guide and target strand and tends to be significantly different, depending on whether the target strand participates or not. It is conceivable that the open-close motion of the PAZ loop is essential for the uptake of siRNA duplex, and the propagation of the guide and target strand may also determine the release of passenger strand cleavage products. For the Ago_S08D model, similar motions were found in PC2 and PC3, which means that the PAZ loop moves with smaller eigenvalues and thereby higher frequencies. To confirm the open-close motion, we determined the distance between the most flexible residue in the PAZ loop and the active site. The open-close ranges vary from 30 Å to 57 Å along this indicator (Fig. 3C) for the Ago_Native model. A similar motion was also observed for the Ago_S08D model but with a slightly smaller cycle. The other three models do not exhibit similar motions and the distances change little. On the other hand, there is no obvious motion for the PIWI loop around 490, which has high RMSF; this means that it behaves randomly.

Change in binding affinity after isoNA modifications

The binding free energy of RISC/ssRNA indicates the release obstacle of the product after cleavage of the passenger strand. After isoNA modifications, the binding free energy decreases for Ago_S08D, whereas those of the other three modifications (Ago_S08L, Ago_S09D and Ago_S09L) increase (Table 1). The activation of RISC may become easier for Ago_S08D due to the easier discarding of the passenger strand, whereas the other three isoNA modification strategies prevent the formation of active RISC. The difference may be related to the motion of the PAZ loop, where the channel with S08D involved closed complex more than the native complex (Fig. 3) and then inhibited the interaction between S08D and Ago2 protein.

Antiviral effects of D-/L-isoNA incorporation at position 8 of passenger strand

Then, the difference between the silencing activities of 8D and 8L was further investigated *via* the downstream antiviral effect. Human herpes simplex virus type 2 (HSV2) belongs to the alpha herpesvirus subfamily and infection with HSV2 produces high morbidity and exhibits broad prevalence, long latency, and difficult curability. To date, no preventive vaccines or effective therapeutic drugs for recurrent infections are available.[21] Enterovirus 71 (EV71) is a positive single-stranded RNA virus belonging to the family of Picornaviridae, which is known to cause hand, foot and mouth disease (HFMD) in young children and can lead to the development of severe

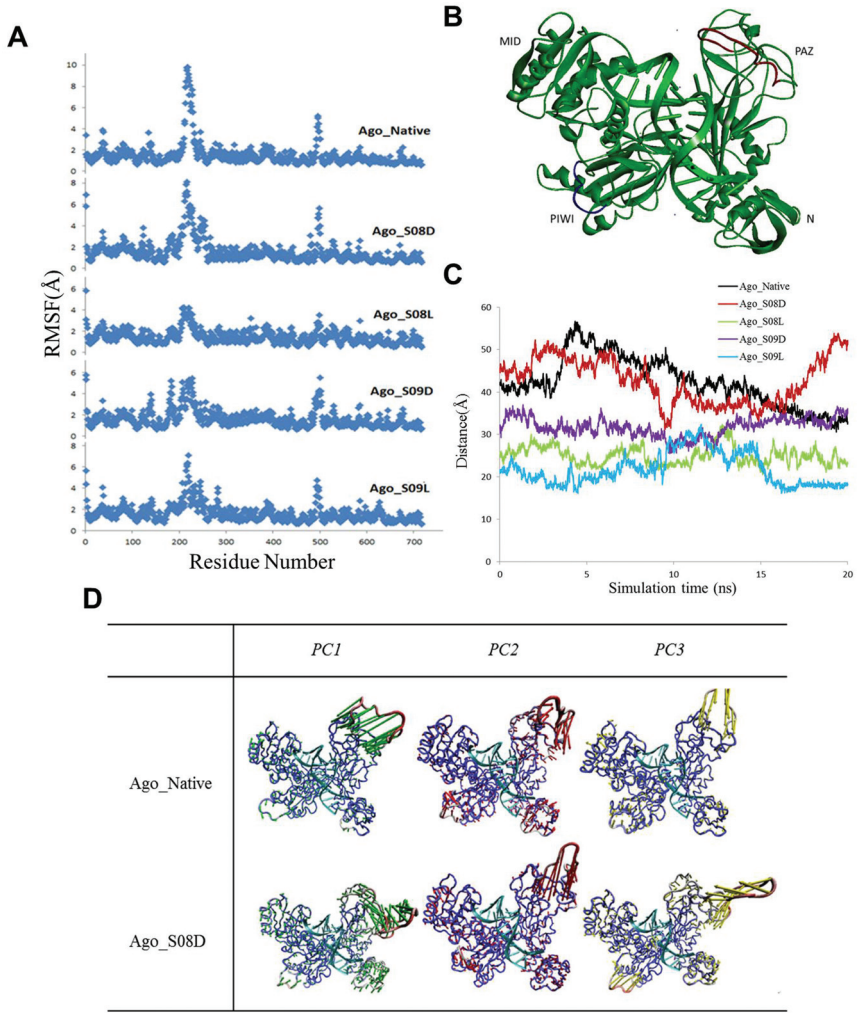

Fig. 3 Stability of the Ago/siRNA complexes. (A) RMSF of each residue in the Ago/siRNA complexes for the last 20 ns; (B) Ago/siRNA complex of Ago_Native model. The red loop refers to the first RMSF peak that appears around residue 220, and the blue loop refers to the second RMSF peak that appears around residue 490; (C) distances between the most flexible residue and the active site of each model during the simulation; (D) the first three principal components (PCs) of Ago_Native and Ago_S08D models during the simulation period.

Table 1 The binding free energies of Ago/siRNA and RISC/ssRNA for each of the models (kcal mol^{-1})

	Ago/siRNA	RISC/ssRNA
Ago_Native	−587.7944 ± 25.5832	−254.2087 ± 20.9272
Ago_S08D	−567.7166 ± 24.0868	−246.0320 ± 17.8012
Ago_S08L	−603.6906 ± 32.4930	−282.1824 ± 24.5516
Ago_S09D	−610.9651 ± 22.4295	−277.2535 ± 15.9013
Ago_S09L	−598.7532 ± 25.6560	−278.9986 ± 19.8106

neurological diseases in some patients, especially children. To date, the treatment and control of EV71 infection are only symptomatic due to the lack of effective medications and unavailability of a prophylactic vaccine.[22] The inhibition of MEK has been studied as the most effective way of investigating the importance of the MAPK cascade in various cellular physiological and pathological processes, including HSV2 and EV71 infection. Herein, we studied the anti-HSV2 and anti-EV71 effects of siMek1 with modification by D/L-isoA at position 8 of the passenger strand by western blotting, virus titration and morphological analysis. To further determine the anti-viral effect of modified siMek1s on the activation of ERK by HSV2 or EV71, HEK293 cells or RD cells were transfected with siRNAs and then infected with HSV2 or EV71, respectively. As shown in Fig. 4A and B, siMek1s effectively silenced the expression of MEK1 and viral gB protein. And, S08D had a better antiviral effect than either the native sequence or S08L, which is in accordance with the former results of silencing activity evaluation.

As one of the most important indices of viral replication, viral titer reflects the release of the live virus in the supernatant of cells infected with the virus. To investigate the influence of D-/L-isoNA-modified siRNAs in HSV2 replication,

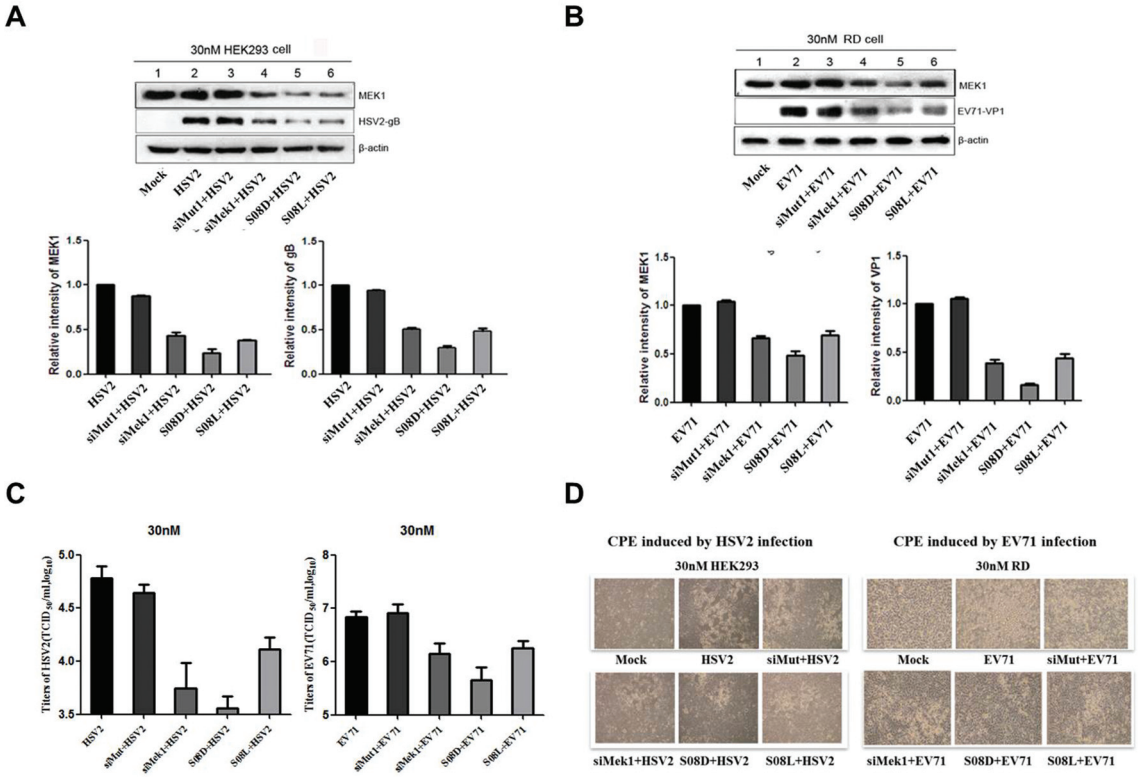

Fig. 4 Antiviral effects of D-/L-isoNA incorporation at position 8 of passenger strand. (A) and (B) Anti-HSV2 and anti-EV71 results of D-/L-modified siMek1s. The experiments were performed as described in Fig. 1 except for virus infection with an MOI of 1.5. Cell lysates that were collected at 24 h p.i. were assayed for viral protein expression by western blot with monoclonal antibodies specific to HSV2 gB protein or EV71 VP1 protein. Quantification of the gB band and VP1 band was normalized by densitometric scanning of actin using the Band Leader software (version 3.0). The relative intensity of gB and VP1 on the *y*-axis is represented by the percentage of the intensity of mock transfection (100%). The data are the average of three independent experiments and error bars denote the standard deviations. (C) Viral titer of HSV2 and EV71 after incubation with D-/L-isoNA-modified siMek1s. HEK293 cells were infected with HSV2 at an MOI of 1.5. Cells and medium were collected separately at different time points. Virus titers in the medium were measured by plaque assay. Data shown are means ± standard deviations (n = 3). The titers on the *y*-axis represent logarithmic values. (D) CPE results with HSV2 and EV71 infection after incubation with D-/L-isoNA-modified siMek1s. Cells were transfected with modified siRNAs (30 nmol of each) and infected at 44 h post-transfection with 1.5 MOI of HSV2. The effects of modified siRNAs on CPE were examined from 8 h p.i. and images were obtained at 24 h p.i.

HEK293 cells transfected with siMek1s were infected with HSV2, whereas RD cells were infected with EV71 and compared with control cells that were infected with HSV2 or EV71 alone, and then the virus production was examined. As shown in Fig. 4C, in the cells that were transfected with 30 nM siRNAs, HSV2 titers were markedly inhibited as compared to control cells that were infected with HSV2 or EV71 alone. Although not as obviously as HSV2, EV71 titers were also inhibited by siMek1s. Moreover, an enhanced anti-viral effect can be seen in S08D compared with unmodified siRNA and S08L.

To determine the effects of siMek1s on the cytopathic effect (CPE) of HSV2 and EV71, HEK293 cells or RD cells that were transfected with siMek1s were infected with HSV2 and EV71 and then monitored by phase-contrast microscopy every 12 h for 3 days p.i. In this experiment, mock infection and viral infection were used as controls. As shown in Fig. 4D, at 24 h, p.i. cells that were transfected with 30 nM siMek1s manifested considerably less CPE as compared to virus and siMut1 controls. Notably, S08D also exhibited less CPE than the others. The virus titer that was observed in the supernatant further confirmed that modification with D-isoNA displayed some potency-enhancing effect at passenger strand position 8, which could be applied in anti-HSV2 and EV71 therapy.

Discussion

Generally, during the process of RNA interference, the cleavage of the passenger strand caused by Ago2 protein occurs between nucleotide 9 and nucleotide 10. Chemical modifications and mismatches located at these two sites are able to interfere with the cleavage process by disturbing the approach of and interaction between cleavage-related residues in the Ago2-PAZ domain and the phosphodiester bond between nucleotide 9 and nucleotide 10. As a result, the silencing activity of modified siRNA would also be reduced.[11] In this report, we also found that irrespective of the incorporation of

D-isoNA or L-isoNA at position 9, the silencing efficiency of modified siRNA was reduced markedly, which is in consistency with other modification strategies. However, chemical modifications at other positions usually have no obvious influence on the cleavage process of the passenger strand.[11] However, we found that D-isoNA and L-isoNA modification next to the cleavage-related site could also affect the cleavage process. Interestingly, D-isoNA and L-isoNA modification introduce considerably opposite influences on the silencing efficiency when the modification occurs at position 8 of the passenger strand.

According to the cleavage kinetics experiment, the passenger RNA strand with modification by L-isoNA was cleaved considerably slower than the unmodified passenger strand at the same position. Based on our previous reports,[18] L-isoNA modification may introduce dramatic alterations in regional conformation not only at the incorporation site, but also around the incorporation site. Therefore, when L-isoNA modification was placed next to the nucleotide 9, it also disturbed the tight interaction between the cleavage-related residues and the corresponding phosphodiester bond. Although in the direct cleavage kinetics test, the passenger RNA strand with D-isoNA modification at position 8 exhibited no difference from the unmodified passenger strand; they exerted quite different influences on the vibration frequency of the Ago2-PAZ domain in the molecular dynamics simulation. This may also be due to the slight alteration in regional conformation around the insertion site caused by modification with D-isoNA. However, study on the precise mechanism of the enhanced vibration frequency of the Ago2-PAZ domain is still ongoing, and to the best of our knowledge, no modification strategy has enhanced the silencing activity by increasing the movement frequency of the PAZ domain. Although the degree of activity enhancement was not quite dramatic, it provided us with more accurate knowledge about the RNA interference process. Our study also reminds us that D-isoNA and L-isoNA, as a pair of chemical tools, could exert quite opposite influences on the interaction between proteins and nucleotides, and they can be applied widely in mechanism studies in the future.

Experimental

Solid-phase synthesis of RNA oligonucleotides

Synthesis of RNA oligonucleotides was carried out at the 1 μmol scale using an Applied Biosystems 394 DNA synthesizer according to regular phosphoramidite chemistry. 2′-OTBDMS-protected D- and L-isoNA phosphoramidite monomers were synthesized as previously reported[18] and then the D-/L-isoNA phosphoramidite monomers were inserted singly into the siRNA sequence at the modified position targeting MEK1 (Fig. 1B). Furthermore, an extended coupling time of 900 seconds was used for D-/L-isoNA phosphoramidites instead of the standard coupling time of 600 seconds that is used for the four standard 2′-OTBDMS-protected RNA phosphoramidites (A^{Bz}, C^{Ac}, G^{Ac} and U) due to the steric effect of isoNA phosphoramidites. Cleavage and deprotection of the oligomers were performed in concentrated ammonia at 55 °C for 24 h and the TBDMS group was removed by treatment with Et_3N/HF in anhydrous DMSO. The crude product was purified by anion-exchange high-performance liquid chromatography (Dionex DNAPac PA200, 9 × 250 mm) using a linear gradient of 12.5%–40% eluent A for 40 min. A solution of 0.02 M Tris-$HClO_4$ in 10% CH_3CN, pH = 8, was used as eluent B, and 0.4 M $NaClO_4$ in eluent B was used as eluent A. Then, the purified oligonucleotides were desalted by a Sephadex G25 column. The purity and identity of the oligonucleotides were confirmed by ion-exchange chromatography and MALDI-TOF MS, respectively, and all single strands were purified by HPLC to >90% purity. Finally, the pure oligonucleotides were lyophilized and stored at −40 °C.

Antibodies

Antibodies were purchased from Cell Signaling Technology (anti-MEK1), EastCoast Bio (anti-HSV gB monoclonal antibody), Abcam (polyclonal anti-EV71 VP1) and Santa Cruz Biotechnology (anti-β-actin).

Cell culture

Rhabdomyosarcoma (RD) cells and human embryonic kidney (HEK) 293 cells were grown in Dulbecco's modified Eagle's medium (DMEM, GIBCO) supplemented with 2% or 10% heat-inactivated fetal bovine serum (FBS, GIBCO) at 37 °C in a 5% CO_2 atmosphere in a humidified incubator.

Virus infection

Monolayers of RD or HEK293 cells at 70%–80% confluency were starved and infected with strain 333 of HSV2 and wild-type EV71 (EV71-BC08 strain) at various multiplicities of infection (MOI). After 1 h at 37 °C, the inoculum was removed and incubation was continued in DMEM containing 2% FBS at 37 °C for viral growth. Supernatants that were collected at different time points post-infection (p.i.) were clarified by centrifugation (2000*g*). Virus titers were determined by plaque assays carried out in triplicate. Viruses were inactivated by UV-irradiation for 30 min using a Phillips TUV 30 W bulb at a distance of 17 cm with occasional agitation, and then blind-passaged for three generations to confirm the loss of replicative capacity.

siRNA and transient transfection

For siRNA transfection, the INTERFER in reagent (Polyplus-transfection) was used according to the manufacturer's instructions. RD cells or HEK293 cells were grown in 12-well plates to 40% confluency. Cells were then transfected with 30 nM specific siRNAs and incubated for the indicated number of hours. The medium was then replaced by DMEM containing 1% FBS and the cells were starved for 8 h.

Morphological analysis

HEK293 cells were examined following infection by HSV2 and EV71 at 12 h intervals post-infection for cytopathic effects (CPE) using phase-contrast microscopy.

Western blotting analysis

Cells were lysed in a buffer containing 20 mM Hepes (pH 7.4), 100 mM NaCl, 5 mM EDTA (pH 7.4), 1 mM Na_3VO_4, 30 mM NaF, 5% glycerol, 0.1% SDS, 1% Triton X-100, 10 mM *p*-nitrophenyl phosphate, and 1 mM glycerophosphate, supplemented with complete protease inhibitors (Roche). Cell lysates were obtained by centrifugation at 4 °C and 13 000 rpm and protein concentrations were determined using the Bicinchoninic Acid Protein Assay Kit (Pierce). Proteins were resolved onto sodium dodecyl sulfate-polyacrylamide gel electrophoresis (SDS-PAGE) gels and transferred to PVDF membranes (Millipore). The membrane was blotted with specific primary antibodies, as indicated in the figure legends, followed by incubation with secondary antibodies conjugated with horseradish peroxidase and developed with an enhanced chemiluminescence substrate (ECL) or SuperSignal West Femto Maximum Sensitivity Substrate (Pierce).

Real-time quantitative PCR (qPCR)

Viral RNAs from supernatants were prepared using Trizol reagent (Invitrogen). Then, 1 μg total RNA was reverse transcribed into cDNA using the RevertAid First Strand cDNA synthesis kit (Thermo Scientific). A quantitation standard curve was obtained using seven 10-fold serial dilutions of recombinant plasmid standard DNA, which contained sequences derived from the gB gene of HSV2 and the VP1 gene of EV71, varying from 1×10^3 to 1×10^9 copies. Real-time quantitative PCR (qPCR) was performed by targeting the gB gene and VP1 gene in 96-well plates using the Roche LightCycler 480 system. Each 20 μL reaction mixture contained 10 μL 2× SYBR Green Supermix, 20 nM target gene primer mix, and 20–50 ng cDNA template. The PCR reaction was set up as follows: initial denaturation step at 95 °C for 10 min, followed by 40 cycles of 30 s at 94 °C, at 55 °C for 30 s and at 72 °C for 30 s. Quantified results for the experimental samples were extrapolated from the standard curve, with all experimental samples being run in triplicate.

Molecular structures of Ago/siRNA complex

Eukaryotic Ago2 protein crystal structures were as reported,[4,5] whereas siRNA double helixes are not involved in the structures. Owing to the high structural similarity of the Ago family, Ago protein from *T. thermophilus* was used as a substitute. There are many *T. thermophilus* Ago proteins in the Protein Data Bank such as 3HJF, 3HK2, 3HM9, 3HVR, 3HO1[23] and 3F73.[24] Ago protein from 3HVR was used because there are no mutations and mismatches and there are two Mg^{2+} ions in the active site. The total nucleotide part from 3HK2 was used after the overlap of the Ago proteins in 3HVR and 3HK2, in which the RMSD of the same guide and target nucleotides (27 nt) between 3HVR and 3HK2 is 1.54 Å. Finally, some processes were carried out to make the siRNA available for the following molecular simulation, which included changing the DNA guide strand to an RNA guide strand, mutating the nucleotide sequence and modifying a specific nucleotide to an isonucleotide according to Fig. 1B. All the operation was performed in Discovery Studio 3.0.

Molecular dynamics simulation

All the molecular dynamics simulations were carried out with Amber 11, and the Amber 10 force field was used. Structures were solvated in a periodic truncated octahedral water box. The minimum distance between the complex and the box wall was 10 Å. The TIP3P water model was applied and sodium ions were placed to neutralize the system. Bonds linking hydrogen atoms were restrained by the SHAKE algorithm. The particle mesh Ewald (PME) method was used to calculate the electrostatic interaction. Minimization of the systems consisted of two stages: at first, 5000 steps of steepest descent and conjugate gradient, respectively, were performed to avoid contact between water molecules by constraining the Ago/siRNA complex. Then, the whole system was minimized under 5000 steps of steepest descent and conjugate gradient. After minimization of the solvated system, the general heating-equilibrium-production pipeline was performed on each structure. The heating process was carried out for 20 ps from 0 K to 300 K with 10 kcal mol^{-1} $Å^{-2}$ harmonic constraint under the NVT ensemble. The following equilibrium process lasted for 100 ps when the harmonic constraint was reduced to 0 gradually under the NPT ensemble. Finally, 24 ns production was conducted under the NPT ensemble and the final 20 ns trajectory was used for analysis. The integration time step was 1 fs and the coordinate was saved every 10 ps.

Principal component analysis

To observe the dominant motions of functional domains of Ago protein, principal component analysis (PCA)[25] was carried out using AmberTools 1.5. First, the coordinate covariance matrix of Ago protein was built up for each complex. Then, the eigenvectors and eigenvalues of the covariance matrix were calculated by diagonalizing the matrix. The eigenvectors represent the collective motions of the Ago domains, whereas the corresponding eigenvalues suggest the importance of the motions. In this study, the three most important motions were selected and projected onto the trajectory. The extreme projection of each motion was used to indicate the directions of the functional domains.

MM/PBSA binding free energy calculation

The binding free energy between a ligand and a receptor is calculated by the following equation:

$$\Delta G_{b,s} = \Delta G_{b,v} + \Delta G_{s,c} - (\Delta G_{s,l} + \Delta G_{s,r})$$

where $\Delta G_{b,s}$ and $\Delta G_{b,v}$ are the binding free energies in solution and vacuum, whereas $\Delta G_{s,c}$, $\Delta G_{s,l}$ and $\Delta G_{s,r}$ are the solvation free energies for the complex, ligand and receptor. $\Delta G_{b,v}$ consists of interaction energy between the ligand and the receptor, whereas sometimes an entropy contribution is also taken into consideration. Solvation free energy is composed of an electrostatic part and a hydrophobic part. In this study, the binding free energies of RISC/ssRNA for Ago/siRNA

complexes were calculated using the MM/PBSA method by the MMPBSA.py module in AmberTools 1.5. Because the differences between complexes are only the isonucleotides, the entropy contribution is neglected.

Acknowledgements

This study was supported by the Ministry of Science and Technology of China (Grant No. 2012AA022501, 2012CB720604, 2013CB966800, 2013CB966802) and the National Natural Science Foundation of China (Grant No. 20932001, 21377085).

Notes and references

1 A. Fire, S. Xu, M. K. Montgomery, S. A. Kostas, S. E. Driver and C. C. Mello, *Nature*, 1998, **391**, 806–811.
2 S. M. Elbashir, J. Harborth, W. Lendeckel, A. Yalcin, K. Weber and T. Tuschl, *Nature*, 2001, **411**, 494–498.
3 A. J. Hamilton and D. C. Baulcombe, *Science*, 1999, **286**, 950–952.
4 S. M. Elbashir, W. Lendeckel and T. Tuschl, *Genes Dev.*, 2001, **15**, 188–200.
5 P. D. Zamore, T. Tuschl, P. A. Sharp and D. P. Bartel, *Cell*, 2000, **101**, 25–33.
6 W. Filipowicz, *Cell*, 2005, **122**, 17–20.
7 H. W. Wang, C. Noland, B. Siridechadilok, D. W. Taylor, E. Ma, K. Felderer, J. A. Doudna and E. Nogales, *Nat. Struct. Mol. Biol.*, 2009, **16**, 1148–1153.
8 K. Miyoshi, H. Tsukumo, T. Nagami, H. Siomi and M. C. Siomi, *Genes Dev.*, 2005, **19**, 2837–2848.
9 K. Kim, Y. S. Lee and R. W. Carthew, *RNA*, 2007, **13**, 22–29.
10 X. Ye, N. Huang, Y. Liu, Z. Paroo, C. Huerta, P. Li, S. Chen, Q. Liu and H. Zhang, *Nat. Struct. Mol. Biol.*, 2001, **18**, 650–657.
11 P. J. Leuschner, S. L. Ameres, S. Kueng and J. Martinez, *EMBO Rep.*, 2006, **7**, 314–320.
12 H. Addepalli, Meena, C. G. Peng, G. Wang, Y. Fan, K. Charisse, K. N. Jayaprakash, K. G. Rajeev, R. K. Pandey, G. Lavine, L. Zhang, K. Jahn-Hofmann, P. Hadwiger, M. Manoharan and M. A. Maier, *Nucleic Acids Res.*, 2010, **38**, 7320–7231.
13 H. W. Yu, L. R. Zhang, J. C. Zhou, L. T. Ma and L. H. Zhang, *Bioorg. Med. Chem.*, 1996, **4**, 609–614.
14 H. Y. Zhang, X. J. Wu, H. W. Yu, L. T. Ma and L. H. Zhang, *Chin. Chem. Lett.*, 1996, **12**, 1089–1090.
15 F. Wang, Y. Chen, Y. Huang, H. W. Jin, L. R. Zhang, Z. J. Yang and L. H. Zhang, *Sci. China Chem.*, 2012, **55**, 1–10.
16 Z. L. Wang, J. F. Shi, H. W. Jin, L. R. Zhang, J. F. Lu and L. H. Zhang, *Bioconjugate. Chem.*, 2005, **16**, 1081–1087.
17 (*a*) J. Zhang, Y. Chen, Y. Huang, H. W. Jin, R. P. Qiao, L. Xing, L. R. Zhang, Z. J. Yang and L. H. Zhang, *Org. Biomol. Chem.*, 2012, **10**, 7566–7577; (*b*) Z. S. Li, R. P. Qiao, Q. Du, Z. J. Yang, L. R. Zhang, P. Z. Zhang, Z. C. Liang and L. H. Zhang, *Bioconjugate. Chem.*, 2007, **18**(4), 1017–1024.
18 Y. Huang, Z. Chen, Y. Chen, H. Zhang, Y. C. Zhang, Y. L. Zhao, Z. J. Yang and L. H. Zhang, *Bioconjugate. Chem.*, 2013, **24**, 951–959.
19 L. Z. Yu, B. Xiong, W. X. Gao, C. M. Wang, Z. S. Zhong, L. J. Huo, Q. Wang, Y. Hou, K. Liu, X. J. Liu, H. Schatten, D. Y. Chen and Q. Y. Sun, *Cell Cycle*, 2007, **6**, 330–338.
20 H. Zhang, H. Feng, L. Luo, Q. Zhou, Z. Luo and Y. Peng, *Virus Res.*, 2010, **150**, 22–27.
21 J. M. Steinbach, C. E. Weller, C. J. Booth and W. M. Saltzman, *J. Controlled Release*, 2012, **162**, 102–110.
22 B. Premanand, T. K. Kiener, T. Meng, Y. R. Tan, Q. Jia, V. T. Chow and J. Kwang, *Antiviral Res.*, 2012, **95**, 311–315.
23 Y. Wang, S. Juranek, H. Li, G. Sheng, G. S. Wardle, T. Tuschl and D. J. Patel, *Nature*, 2009, **461**, 754–761.
24 Y. Wang, S. Juranek, H. Li, G. Sheng, T. Tuschl and D. J. Patel, *Nature*, 2008, **456**, 921–926.
25 A. Amadei, A. B. Linssen and H. J. Berendsen, *Proteins*, 1993, **17**, 412–425.